

# Collective motion of run-and-tumble particles drives aggregation in one-dimensional systems.

Christian Vanhille Campos,<sup>\*</sup> Francisco Alarcn Oseguera,<sup>†</sup>  
 Ignacio Pagonabarraga,<sup>‡</sup> Ricardo Brito,<sup>\*</sup> and Chantal Valeriani<sup>§</sup>  
 (Dated: March 25, 2021)

We numerically study a one-dimensional system of self-propelled particles on a lattice where the state of each particle is given by its moving direction (left or right) and its position on the lattice. Particles obey run-and-tumble dynamics and interact with each other via excluded volume. Besides particle motion, we consider the collective motion of aggregates towards the direction dictated by the majority of their constituents (in a momentum-conservation manner). Our results show that this non-equilibrium system reaches a stationary regime with very distinct states of aggregation that depend on the tumbling rate and the density. We demonstrate that these states are characterized by the existence of moving clusters of jammed particles separated by a gas of free-moving particles in constant dynamical exchange. Thus, we prove that each state of aggregation presents very different cluster size distribution and site-to-site occupancy correlation functions appearing to evolve continuously from one state to the other as the tumbling rate and the density vary. We believe our results to be of key relevance to understand that no alignment interactions or attractive forces are needed for self-organization, aggregation and collective motion to emerge in a suspension of active particles.

**Usage:** Secondary publications and information retrieval purposes.

**PACS numbers:** May be entered using the `\pacs{#1}` command.

**Structure:** You may use the `description` environment to structure your abstract; use the optional argument of the `\item` command to give the category of each item.

## I. INTRODUCTION

Active matter encompasses any kind of soft matter system where particles consume energy at the individual level to achieve motion, thus leading the system to be intrinsically out of equilibrium even in the absence of applied forces and external fields [1, 2]. Such characteristics lead to the appearance of common properties to any active matter system [3] such as: the emergence of collective structures with qualitatively different behaviors from individual ones[4, 5], out-of-equilibrium phase transitions from disordered to ordered systems and vice-versa (*coarsening*[6] and *clustering*[7–10]), pattern formation at the mesoscale[11–13], special mechanical and rheological properties[14–16], novel fluctuation statistics

with respect to equilibrium and other non-equilibrium systems[17–20].

To understand, predict and even reproduce these active matter features, the most common procedure is to take a bottom-up approach and, from the individual behavior of the constitutive parts, describe the collective properties of a system by means of statistical physics tools. Individual behaviors, however, are in general quite complicated and a first modelling step is needed, thus boiling down the elements of a system to moving particles obeying few straightforward rules that replicate the observed dynamics while keeping the number of free parameters fairly low [3].

Some models define the particles' dynamics from the speed's direction, establishing aligning rules leading to collective organized motion [21, 22], while others focus on the speed, making particles moving slower where the density is higher, leading to aggregation events (Motility Induced Phase Separation) [23, 24]. An extreme case of MIPS is Excluded Volume (EV), which enforces that two different particles cannot overlap, also leading to aggregation events when particles are locally trapped together. A simple implementation of EV is the Persistent Exclusion Process (PEP) introduced in Ref.[25]. This consists in a discrete on-lattice model of self-propelled particles obeying run-and-tumble dynamics with the only added condition that two different particles cannot occupy the same lattice site at the same time. Thus, the whole dynamics can be expressed only in terms of two parameters: the tumbling rate  $\alpha$  and the number density  $\phi$ . Interestingly, this is enough to detect clustering and ordering in the system. This model has later been expanded to a

<sup>\*</sup> Departamento de Estructura de la Materia, Física Trmica y Electrónica, Facultad de Ciencias Físicas, Universidad Complutense de Madrid, 28040, Madrid, Spain

<sup>†</sup> Departamento de Estructura de la Materia, Física Trmica y Electrónica, Facultad de Ciencias Físicas, Universidad Complutense de Madrid, 28040, Madrid, Spain; Departamento de Ingeniería Física, División de Ciencias e Ingenierías, Universidad de Guanajuato, Loma del Bosque 103, 37150 Len, Mexico.

<sup>‡</sup> Departament de Física de la Matèria Condensada, Universitat de Barcelona, 08028 Barcelona, Spain.; Universitat de Barcelona Institute of Complex Systems (UBICS), Universitat de Barcelona, 08028 Barcelona, Spain; CECAM, Centre Européen de Calcul Atomique et Moléculaire, cole Polytechnique Fédérale de Lausanne, Batochime, Avenue Forel 2, 1015 Lausanne, Switzerland

<sup>§</sup> Departamento de Estructura de la Materia, Física Trmica y Electrónica, Facultad de Ciencias Físicas, Universidad Complutense de Madrid, 28040, Madrid, Spain; cvaleriani@ucm.es

finite maximum occupation number per site [26], leading to the existence of three different phases (gas, *clusters* and solid). Recently, the PEP model has also been used to explain wetting transitions in bacterial populations [27].

Following a similar idea, there exists a number of studies on pattern emergence and self-organization in active systems resulting from the competition between self-propulsion and excluded volume interactions reporting the effects of alignment interactions [28] or attractive forces [8, 29] both in 1D and 2D. In particular, Ref.[29] gives a very interesting example where simple attraction rules and excluded volume lead to complex aggregation dynamics even in one dimension. Indeed, not only does the model presented in Ref.[29] allow for aggregation, but, more importantly, leads to the emergence of motile clusters. It is thus one of the few existing modelling attempts to describe collective migration and swarming clusters without alignment interactions.

Collective particles' motion is indeed a key element of active matter, often observed in natural phenomena and of which there exist plenty of experimental studies [30, 31]. Most often, such dynamics are replicated via alignment interactions between particles as in the Vicsek model [21]. There is evidence, however, that in a one-dimensional system of self-driven particles, such alignment is not needed to display collective aggregated motion, also achieved with attraction forces [29].

It has been recently shown that self-propelled droplets, confined in a one dimensional micro-fluidic channel, experience a collective dynamics characterised by flocks of neighbouring clusters. This phenomenon is the result of the interplay between velocity fluctuations and the absence of Galilean invariance [32]. Cluster condensation takes place as a transient phenomena which slows down the dynamics, before the system settles into a homogeneous aligned phase.

In the present work, we introduce an even simpler on-lattice one-dimensional model with no interactions except for the excluded volume, as in Ref.[25], but explicitly considering collective motion of aggregates, inspired by momentum conservation. For a wide range of tumbling rates  $\alpha$  and particle densities  $\phi$  these dynamics generate moving clusters of jammed particles separated by dilute regions of free moving particles. We observe a striking different behavior depending on the ratio between  $\alpha$  and  $\phi$ , with either small or big clusters, leading to a contrasting state of aggregation. To understand this phenomenon we probe the cluster size distribution in the stationary regime as well as the evolution towards this steady state (namely the reduction and stabilization of the total number of clusters in the system). We also analyze the dependence of the state of aggregation on the system's parameters by means of numerical aggregation parameters (similar to the classical order parameters used to study phase transitions), such as the fraction of jammed particles or the normalized average cluster size in the stationary regime. Finally, we also compute site-to-site spatial

occupancy correlations, which present striking differences between the different states of aggregation, and we probe the model for finite size effects.

The paper is structured as follows. In Section II we present the model and discuss the details of the simulation, such as the computation of relevant variables. Results of the simulations are then presented in Section III: see IIIB for results regarding the cluster size distribution, IIIC for the aggregation parameters and IIID for the site-to-site occupancy correlations. Finally, in Section IV we present concluding remarks and in Section VI are included supplementary results.

## II. SIMULATION DETAILS

In this work we consider a one-dimensional realization of the Persistent Exclusion Process (PEP) model as in [25]. The system consists in a lattice of  $L$  sites with a population of  $N$  particles defined by a density  $\phi$  ( $N = \phi L$ ). Particles only move on the lattice and are characterized by their position  $x_i$  and direction of motion  $d_i = \pm 1$ :  $d_i = +1$  if a particle  $i$  moves to the right (in blue in Fig.1) and  $d_i = -1$  if a particle  $i$  moves to the left (in red in Fig.1).

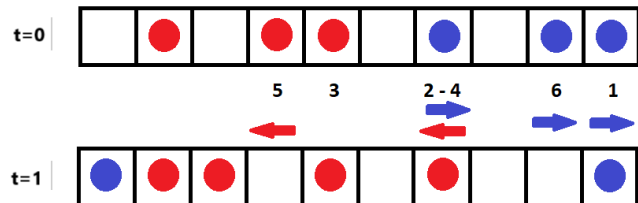


FIG. 1. Visual representation of the system for  $L = 10$  and  $N = 6$  at two consecutive time steps ( $t = 0$ , top row and  $t = 1$ , bottom row). Left-pointing particles are printed in red and right-pointing particles in blue. The numbers indicate the order of updates and the arrows the direction of motion.

Particles move according to the following scheme. Both particles positions and directions of motion are updated over discrete time steps. 1) At each time step  $N$  particles are chosen at random, allowing for repetitions, and are updated sequentially. 2) For each of these, first their direction is allowed to change randomly with tumbling probability  $P_{tumble} = \alpha$ . 3) Each particle then performs a one-site jump in the new direction only if the landing site is empty (excluded volume is enforced). Otherwise, the particle stays in its original position. 4) Finally, periodic boundary conditions are enforced on the system.

In Fig.1 we present an illustrative example of such a system at two consecutive time steps: there are  $N = 6$  particles so 6 particles are updated sequentially, in the order given by the numbers. Note that one particle moves twice (in second and fourth position) while another particle isn't updated during this time step. Note also that

particles pointing to an occupied site don't move (particle updated in third position for example). Finally, note that the particle updated twice ends up on its initial site, since it has changed direction (a tumble occurred) during its second update, before the jump was performed.

In this work we propose a modification to the classic PEP model defined above [25], that now includes moving clusters of particles. To start with, we identify a cluster as any group of two or more neighbouring particles "trapped" in a certain position (with particles at the cluster's boundaries having opposing directions, as in Fig.2).

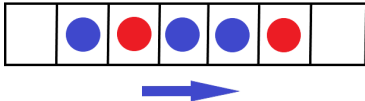


FIG. 2. Visual representation of a five-particle cluster and its resulting jumping direction. Left-pointing particles are printed in red and right-pointing particles in blue. The arrow indicates the resulting cluster jumping direction.

To implement cluster mobility, at each time step: 1) we evaluate whether particles have clustered, 2) we compute the cluster's direction of motion  $D_C$ , summing up each constituting particle's direction of motion  $D_C = \frac{\sum d_i}{|\sum d_i|}$  (where  $d_i$  is the direction of each particle:  $\pm 1$ ); 3) each cluster will move with a given probability  $P_C = \frac{|\sum d_i|}{l}$  (where  $l$  is the length of the cluster), independently of the rest of the dynamics and only once the individual particles have been updated. A visual representation of such cluster move is shown in Fig.2.

Note that when  $\alpha = 0$  our model resembles a TASEP [33] model with an additional cluster move. However, in the rest of the work we will only work with  $\alpha \neq 0$ .

Throughout this work we are particularly interested in characterizing the state of aggregation of the system. To this end, we have used the following analysis tools: the cluster size distribution, the normalized average cluster size  $M$ , the fraction of jammed particles  $J$ , (we use the latter two to build the system's state diagram) and the site-to-site occupancy correlation function.

To measure the cluster size distribution at time step  $t$  ( $P_{l,t}$ ) we compute the number of clusters of size  $l$  at time  $t$  ( $n_{l,t}$ ) and normalize by the total number of clusters at that time.

$$P_{l,t} = \frac{n_{l,t}}{\sum_l n_{l,t}} \quad (1)$$

As expected, the system relaxes to an out-of-equilibrium steady-state with a constant cluster size distribution  $P(l) = \langle P_{l,t} \rangle_t$ , as in the PEP model. Therefore, one needs to wait for the system to reach a steady state in order to be able to measure aggregation. This corresponds to simulating the dynamics over  $T_{max} = 10^8$  and measure the cluster size distribution for  $t \gg 10^4$  at intervals of  $T_{save} = 10^4$  (see Appendix B - Section VIA for details on this).

While the cluster size distribution constitutes a key element in the study of the system, it doesn't provide a quantitative measure of its state of aggregation. This is the reason why we introduce the variable  $J$  corresponding to the average fraction of jammed particles (trapped in clusters) in the steady state. Its physical interpretation is straightforward, as the closer it is to 1 the more aggregated the system will be: if  $J = 1$  all particles are trapped in clusters and there are no free active particles in the dilute regions. On the contrary, if  $J = 0$  all particles are free and no aggregation has occurred.

However,  $J$  by itself isn't sufficient to assess whether the system is in a coarsened or clustered state as  $J$  can be close to 1 independently of the number of clusters. Indeed, ideally, all particles could be trapped in a few clusters of small size (so the system would be in a clustered state) or in a single large cluster (so the system would be in a coarsened state) and  $J$  would still be equal to 1 in both cases. Therefore, to properly determine what state of aggregation the system is in, we need another variable:  $M$ . We define  $M$  as the normalized average cluster size in the steady state ( $M = \frac{1}{N} \sum_l P(l)l$ ), so it ranges from 0 to 1. Again, its physical meaning is very straightforward as the closer it is to 1 the more coarsened the system will be. Since both  $J$  and  $M$  allow to determine the state of aggregation of the system quantitatively they can be interpreted as a sort of order parameters for the aggregation of the system (in a similar spirit to that of classical phase transitions). However, these are not order parameters as we are not dealing with a phase transition in the classical thermodynamics sense, so we will refer to these as aggregation parameters of the system.

Finally, to properly assess the behavior of the system we are also interested in the spatial correlations between particles in the steady-state, which should represent the aggregation effects leading to clustering and coarsening. To this end, we compute the space correlations between particles at a given time  $t$  ( $C_{x,t}$ ) for different time steps in steady state as indicated in Equation 2 and then take the average over these times  $C(x) = \langle C_{x,t} \rangle_t$  for the site-to-site occupation correlation function in the stationary regime.

$$C_{x,t} = \frac{\sum_i s_{i,t} s_{i+x,t}}{N} \quad (2)$$

In Equation 2,  $x$  corresponds to the distance between two particles, ranging from 1 to  $L/2$ ,  $s_{i,t}$  is the occupancy number (1 or 0) of site  $i$  at time-step  $t$  and  $N$  is the total number of particles. The normalization constant is chosen so that  $C_{0,t} = 1$  and periodic boundary conditions are taken into account ( $((i+x)L = i+x-L)$ ).

Finally, to discard finite size effects, we have carefully performed simulations in the range  $L \in [0, 5000]$  (see Appendix A - Section VIB) and concluded that no finite size effects were present. In the remaining of the paper, we will thus restrain ourselves to  $L = 2000$ .

### III. RESULTS

#### A. Qualitative behavior

To get an idea of the qualitative behavior of this model, we start by considering two systems of size  $L = 300$  but with different values of  $\alpha$  and  $\phi$ . The first one is a case with small tumbling rate,  $\alpha = 0.001$ , and density  $\phi = 0.2$ . In the second case the tumbling rate is increased to  $\alpha = 0.05$ , and the density is  $\phi = 0.6$ . In both cases the system is initiated with a random configuration.

The spatio-temporal evolution of both cases at short and long simulation times is presented in Fig.3. It represents the time evolution of particles' trajectories, where the different colours correspond to particles moving to the left (in red) or to the right (in blue). When  $\phi = 0.2$  and  $\alpha = 0.001$ , at short times particles form clusters (top row - panel a) that merge at longer times (top row - panel b) with the system coarsening into a dilute and a dense phase. The same happens when the concentration and the tumbling rate are higher ( $\phi = 0.6$  and  $\alpha = 0.05$ ): at short times particles form clusters (bottom row - panel c) that merge at longer times (bottom row - panel d). The main difference between a lower  $\phi - \alpha$  system (top row) and a higher one (bottom row) is that not only clusters are less dynamic in the former than in the latter case (see how clusters form straighter lined and better defined packs of particles in the top row than the bottom one), but also coarsening is more evident for lower  $\alpha$  (note the single cluster in panel b).

This behavior presents some similarities with the PEP model described in Ref.[25], where particles also show a clustering behavior with a constant dynamical exchange between dense and dilute regions. However, we should also underline significant differences between the two systems. While for the PEP model only small clusters are formed and remain immobile, here the clusters' mobility leads to the formation of much larger clusters, which are formed by merging smaller ones. Such dynamics greatly affect the state of aggregation of the system.

To further characterize the effects of this cluster mobility, we now compute the cluster size distribution, the dependence of the different aggregation parameters (see Section II) on  $\alpha$  and  $\phi$  and the site-to-site occupancy correlations.

#### B. Cluster size distribution

A key tool to understand the system's steady state is the cluster size distribution (defined in Section II). In Figures 4 and 5 we report the cluster size distribution for different tumbling rates and densities. The novel feature of the cluster mobility introduced here is the presence of a peak in the distribution at the value  $l/N = 1$ , indicating the presence of a cluster of size  $l = N$ , that is, a cluster that contains all the particles of the system. Therefore, the system is in a so-called coarsened

state. It thus no longer obeys the probability distribution presented in Ref.[25] where mobility is not present. Moreover, the exponential decay of the cluster probability,  $P(l)$  does not hold anymore as mobility also affects the existence of small clusters.

Together, these two figures show that the system's steady state is more aggregated as the density increases and the tumbling rate decreases, being maximal for  $\alpha \ll \phi$  (coarsening). Therefore, depending on the system parameters  $\alpha$  and  $\phi$ , we distinguish three steady-state regimes: clustering, coarsening and a transition regime.

Concerning the coarsening regime (see for example the top-left panel of Fig.4), we find that for  $\alpha \ll \phi$  the system evolves towards a steady-state of maximum aggregation where all particles get trapped in a single or a few very large clusters (indicated by the peak of  $P(l)$  at  $l/N = 1$ ), surrounded by a very dilute gas of free particles in constant dynamical exchange. Note the two branches of the cluster size distribution (all but the green curve) corresponding to the dense and dilute regions in the system, respectively decaying for small clusters and increasing for large ones.

On the contrary, for  $\alpha \sim \phi$  the system reaches a state of minimum aggregation where clusters dissolve before merging together so that particles are trapped in clusters of very small size surrounded by a dense gas of free particles. This is what we refer to as the clustering regime (see for example the top-right panel of Fig.5). Note here the single decaying branch in the cluster size distribution, which is quite similar, for this parameter set, to that observed in the simple PEP model [25].

Finally, for certain values of the parameters such that  $\alpha \leq \phi$  (see for example the bottom-middle panel of Fig.5) we find that the system behaves in an intermediate way (transition regime), with clusters merging together and increasing in size but dissolving before reaching their maximum size.

On one hand, in Fig.4 we fix the tumbling probability  $\alpha$  and, in each panel, compare the distributions for different densities. Increasing the density, we observe that instead of clusters of any size, the system starts phase separating into a dilute and dense region. Therefore, coarsening seems to be the predominant feature up to a tumbling rate of  $\alpha = 0.010$  beyond which the system mostly forms clusters. When the density is relatively low, the cluster size distribution has an exponential feature resembling that already presented by Soto et al. [25]. Moreover, we also observe the evolution of the system's steady state distribution as  $\alpha$  increases (read panels from left to right and top to bottom), suggesting a maximum value of  $\alpha$  for the existence of coarsening.

On the other hand, in Fig.5 we fix the density  $\phi$  (as opposed to Fig.4) and compare in each panel the distributions for different tumbling probabilities  $\alpha$ . Each column thus corresponds to a different order of magnitude for  $\alpha$  ( $10^{-3}$ ,  $10^{-2}$  and  $10^{-1}$  from left to right) while each row corresponds to a different density (low density at the top and high density at the bottom). We thus observe

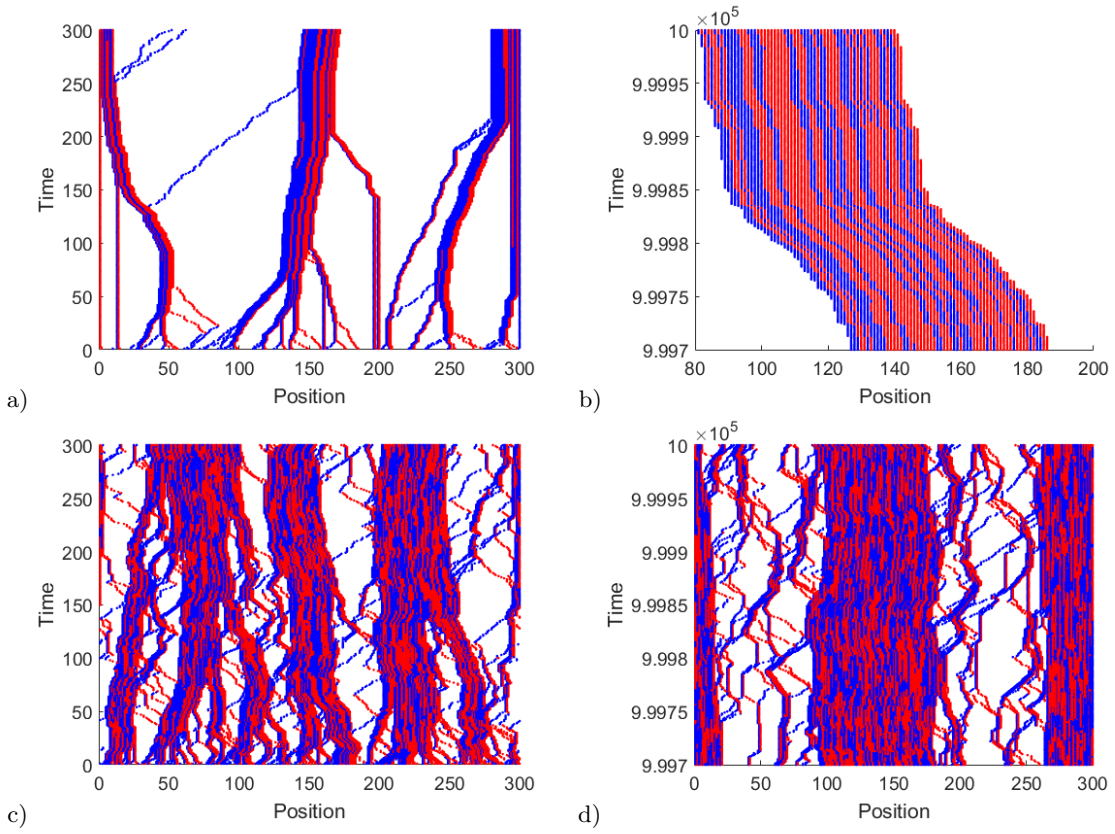


FIG. 3. Spatio-temporal diagrams of a system with  $L = 300$  for  $\phi = 0.2$  and  $\alpha = 0.001$  (top two figures) and for  $\phi = 0.6$  and  $\alpha = 0.05$  (bottom two). Left-pointing particles are printed in red and right-pointing particles in blue.

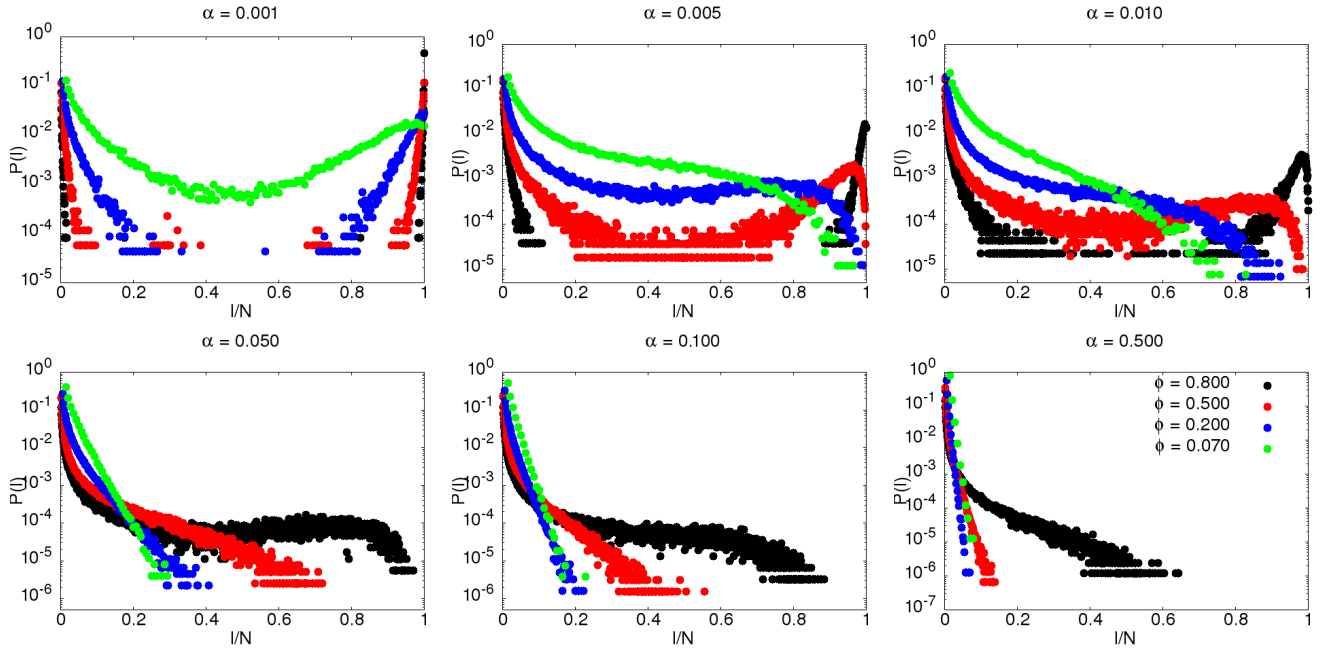


FIG. 4. Cluster size distributions for different parameters in the stationary regime. The different colors correspond to different values of  $\phi$  as shown in the legends. Each panel corresponds to a different value of  $\alpha$ .

that as the tumbling rate  $\alpha$  increases the system gets more dilute, with large clusters disappearing. Indeed, we notice how for  $\phi = 0.07$  (top row) the distribution goes from spanning all cluster sizes to only covering the smallest ones as  $\alpha$  increases. Similarly, for  $\phi = 0.50$  (bottom row) the distribution first presents two distinct peaks for small and large cluster sizes (see left most panel) which slowly merge together as  $\alpha$  increases leading to a curve that first spans all cluster sizes and ends up covering only very small clusters.

### C. Quantitative characterization of the state of aggregation: $J$ and $M$

In this section we analyze the dependence of the two aggregation parameters ( $J$  and  $M$ ) introduced in Section II on the system's parameters, which allow to easily determine the state of aggregation of the system from the  $\{\alpha, \phi\}$  parameter space.

Figure 6a illustrates the dependence of  $J$  on the system's parameters  $\alpha$  and  $\phi$ . We thus observe that, as expected, for a fixed density (see panel a) the system evolves towards a state of full aggregation as the tumbling rate decreases to zero and becomes more dilute as it increases. Note also that the values of  $J$  are consistently higher for all  $\alpha$  as the density increases, with some values of  $\phi$  appearing to forbid a fully dilute system. This is consistent with the results of the cluster size distribution, where we observe that the system approaches the coarsened state as  $\alpha$  decreases (see top row panels in Fig.4).

On the other hand, Fig.6b illustrates the dependence of  $M$  on the system's parameters. We observe here that  $M$  presents a decreasing dependency on  $\alpha$  with consistently higher values for higher  $\phi$  and a similar exponent for all densities (see the parallel slopes). Note however that  $M$  saturates to a minimum ( $M_{min} = 2/N$ ) due to the finite size of the system as  $\alpha$  increases and that this happens at lower  $\alpha$  for lower densities (notice how the green and blue curves in Fig.6 - panel b clearly saturate in the studied range while the red and black keep decreasing), as  $M_{min}$  is higher in these cases. Since the minimum value of  $M$  depends on the system size, meaning that the saturation of the curves for low densities could be avoided by simulating a larger system. Nonetheless, even though  $M$  presents a minimum value due to the finite size of the system, it is important to note that its decay towards that minimum is universal and follows a power-law behavior, as displayed by the parallel straight lines in Fig.6b before saturation.

The aggregation parameters  $J$  and  $M$  thus have a complex dependence on  $\alpha$  and  $\phi$ , which is illustrated in Fig.7. Hence, we can easily determine the state of aggregation of the system using  $J$  and  $M$ : for large  $\phi$  and low  $\alpha$  (top left corner of both panels a and b) coarsening occurs (this corresponds to the coarsening regime presented in Section III B) as  $J$  saturates to 1 (there are none or very few free particles) and  $M$  is maximum (the average

cluster size is large, close to  $N$ ), as also shown in Fig.6. A snapshot of the system in such a state is presented in the bottom panel of Fig.7 - snapshot a), where we observe the single aggregated cluster with no free particles, characteristic of the coarsening regime.

Then, as we move to lower  $\phi$  or higher  $\alpha$ , both  $J$  and  $M$  decrease in value. Note that this decrease is faster and more evident for  $\alpha$  than  $\phi$ , as we can still have high  $J$  and  $M$  for low densities if the tumbling rates are sufficiently low. However,  $J$  and  $M$  don't follow exactly the same behavior and for middle-range values (center of the top two panels in Fig.7)  $J$  is still high while  $M$  is very low, which indicates that the system is in an aggregated clustered state (corresponding either to the clustering regime or the transition regime in Section III B), where there are few free particles but the clusters are small in size. An example of this state of aggregation is illustrated in Fig.7 - bottom panel - b, where we observe the aggregated clustering regime, with a number of relatively large clusters together with some smaller ones and a few free particles.

Finally, for very low density and high tumbling rate (bottom-right part of the top two panels in Fig.7), both  $J$  and  $M$  are close to 0, meaning that most particles are free and the few existing clusters are very small: the system is in its most dilute state of aggregation (corresponding to the clustered regime in Section III B). An example of this is presented in snapshot c of the bottom panel in Fig.7.

### D. Site-to-site occupancy correlation

In order to better characterize the aggregation dynamics we have also computed the site-to-site occupancy correlations  $C(x)$ , which can be understood as the probability that two particles are at a distance  $x$  from each other. Note that  $C(x) \in [0, 1]$  and  $C(0) = 1$ , which means that the closer  $C(x)$  is to 1 the more often two particles are at a distance  $x$  from each other.  $C(x)$  approaching 0 corresponds to the case where there are no two particles at a distance  $x$  in the stationary regime. An important case to consider for comparison is the fully dilute system (uncorrelated occupation of the lattice sites), which leads to  $C(x) = \phi, \forall x$ .

In Figure 8 we present  $C(x)$  for fixed tumbling rates (see different panels) at different densities. We observe that for a fixed  $\alpha$ , correlations are consistently higher for all distances  $x$  as the density increases while always presenting a similar behavior. The general shape of the curve is linked to the tumbling rate, as we can appreciate by comparing the different panels on Fig.8. We thus distinguish three different correlation regimes, which correspond to the different states of aggregation.

First, for a coarsened system (one single large cluster), correlations can be calculated analytically. We find that correlations decrease linearly with the distance  $x$  at a slope that only depends on the density  $\phi$  (as for a single cluster its size equals  $N$ , and it is impossible to find a

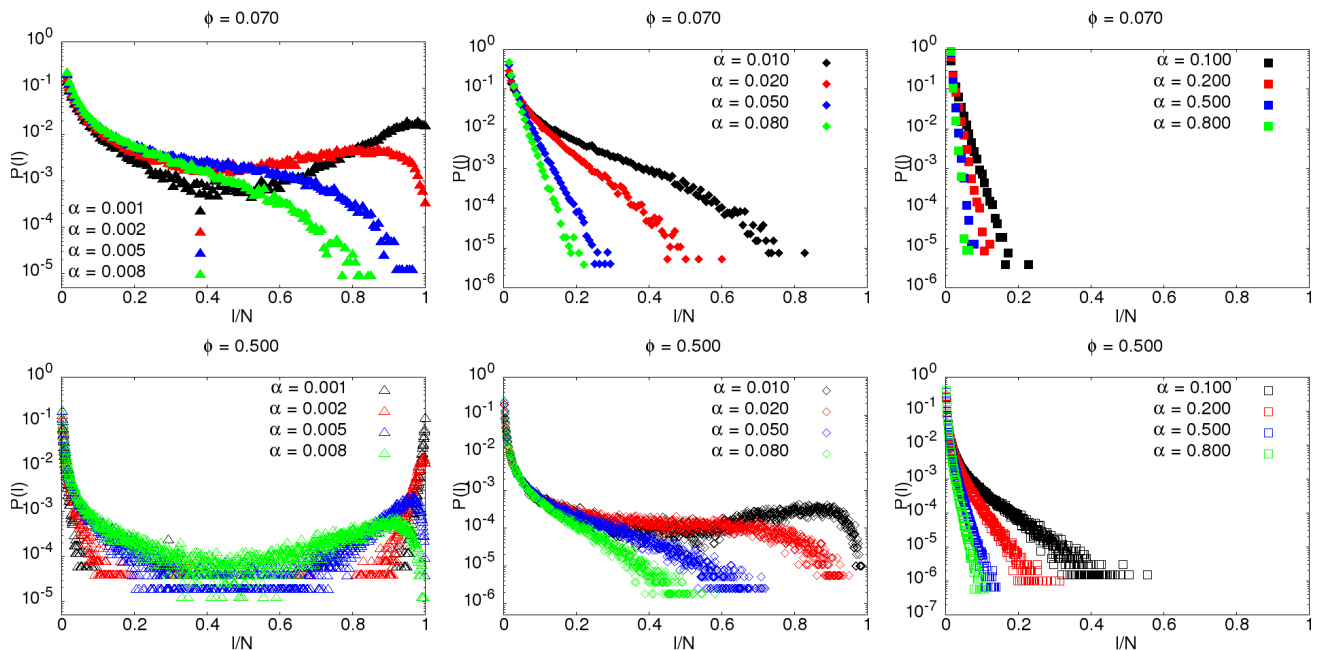


FIG. 5. Cluster size distributions for different parameters in the stationary regime. The different colors correspond to different values of  $\alpha$  which increases by a factor 10 for each subsequent column. The top row corresponds to a low density:  $\phi = 0.07$ . The bottom row corresponds to a high density:  $\phi = 0.50$ .

pair of particles at distances larger than  $N$ ). The exact expression for the correlations in the coarsened regime is  $C(x) = \max(f(x), 0) + \max(f(L - x), 0)$  where  $f(x) = 1 - x/N$ . Therefore, correlations only reach zero for  $\phi < 0.5$  while for  $\phi > 0.5$  they reach a minimum  $C_{min} = 2 - 1/\phi < \phi$  at  $x = L - N$ , as shown in Fig.8 (solid lines). Note how for low  $\alpha$  (top panel) the theoretical curves are indistinguishable from the simulation results for most densities (for  $\phi = 0.07$  there is a slight discrepancy which is due to the fact that this system is not in a perfectly coarsened state, as can be seen in Fig.4 - panel a as well).

On the contrary, for very dilute systems in the clustering regime (see Fig.8 - bottom panel) we find that correlations decay very rapidly with  $x$  towards  $C_{min} = \phi$ , which corresponds to a gas-like uncorrelated system.

Therefore, the system presents two clear types of correlations for the coarsened and dilute regimes, which match very well the type of behavior expected for each of them. Systems in between these two distinct states however, present a variety of shapes in their correlation functions. We expect these shapes to be a result of the convolution of single cluster correlation functions for the different cluster sizes present in the system. Indeed summing the single cluster correlation functions (with a triangular shape shown in the top panel) yields similar decaying behaviors as shown in the middle and lower panel.

Finally, in order to assess how structured the system is from the correlation functions it is interesting to consider the shape these would take for perfectly periodic systems (i.e. in which clusters are spaced out by a constant distance, thus presenting a repeating pattern throughout

the system). Thus, for a system of repeating clusters of size  $l$  and distance  $d$  we would observe a periodic correlation function with a linear profile reaching a minimum at  $x = l$  and then again a maximum at  $x = d + l$  and so on. For systems with a similar but less periodic structure the curve would become noisier. The observed shapes are far from periodic, meaning that there exists little or no structure in the arrangement of clusters, although some systems present a shallow minimum at some distance  $x'$  (see the blue and green curves in the middle panel of Fig.8) which might indicate the existence of a dominating distance between clusters.

#### IV. DISCUSSIONS AND CONCLUSIONS

In our work, we have presented a simple on-lattice one-dimensional model with no interactions except for the excluded volume, as in Ref.[25], but explicitly considering collective motion of aggregates, inspired by momentum conservation. We have implemented both dynamics using an in house code and found that cluster mobility leads to a novel state of maximum aggregation for given parameter values. For a wide range of tumbling rates  $\alpha$  and number densities  $\phi$  these dynamics generate moving clusters of jammed particles separated by dilute regions of free moving particles. We observe a strikingly different behavior depending on the ratio between  $\alpha$  and  $\phi$ , leading to a contrasting state of aggregation.

To understand this phenomenon we have probed the cluster size distribution in the stationary regime as well

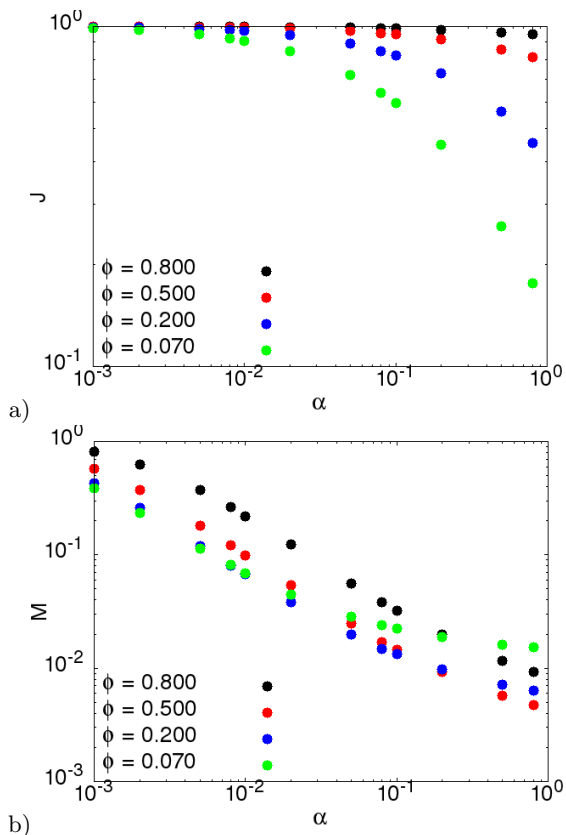


FIG. 6. Dependence of the  $J$  and  $M$  aggregation parameters on  $\alpha$  and  $\phi$  in the steady state. We fix  $\phi$  (see legend) and plot the dependence with  $\alpha$  (x-axis) in log-log scale. Panel a):  $J$  parameter. Panel b):  $M$  parameter.

as the evolution towards this steady state. We have also analyzed the dependence of the state of aggregation on the system's parameters by means of numerical aggregation parameters, such as the fraction of jammed particles or the normalized average cluster size in the stationary regime. Finally, we have computed site-to-site spatial occupancy correlations, which present striking differences between the different states of aggregation, and checked the model for finite size effects.

The system reaches a steady state with a constant cluster size distribution, stabilizing the average number of clusters and with a regular site-to-site occupancy correlation functions. Based on these evidences, we distinguish two contrasting states of aggregation, with a continuous transition phase between them. First, for high tumbling rates and low densities we observe the emergence of a dilute clustered phase, with some particles trapped in dense clusters separated by dilute regions of free particles. Here, the cluster size distribution is only decreasing, with a small average cluster size, and the site-to-site occupancy correlation function falls rapidly towards  $C = \phi$ , corresponding to a perfectly dilute system. Second, for low tumbling rates and high densities we observe the emergence of a highly aggregated coarsened phase, with most particles trapped in one or a few large clusters

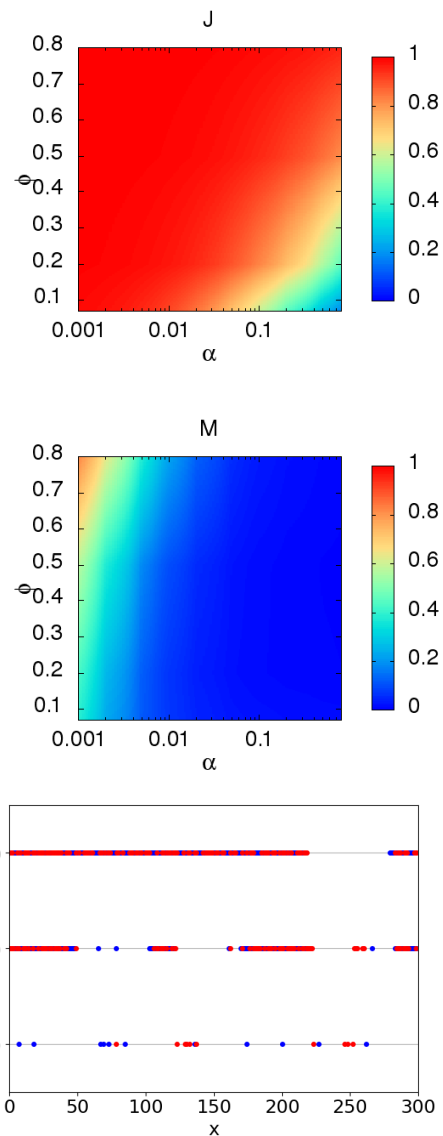


FIG. 7. **Top and middle panels:** Color-coded contour plots representing the dependence of the  $J$  and  $M$  aggregation parameters on  $\alpha$  and  $\phi$  in the steady state. The  $\alpha$  axis is set in logarithmic scale. **Bottom panel:** Snapshots of the system after  $T = 10^6$  time steps for  $L = 300$  and different  $\alpha$ - $\phi$  combinations. a):  $\alpha = 0.001$   $\phi = 0.800$  b):  $\alpha = 0.050$   $\phi = 0.500$  c):  $\alpha = 0.800$   $\phi = 0.070$ .

separated by a gas of free particles at a very low density. Here, the cluster size distribution is decreasing for small sizes and then again increasing for large clusters, usually reaching a maximum for  $l = N$ . The average cluster size is thus very large, while the site-to-site correlation function presents a linearly decreasing behavior as expected to be measured when all particles are trapped in a single cluster.

Even though in our work we present a simple system, we believe it already provides some insight into ag-

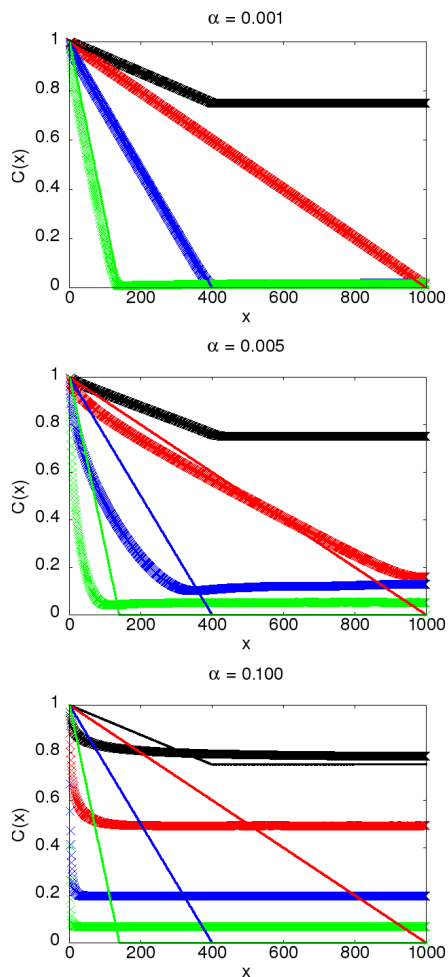


FIG. 8. Space correlations between particles in the steady-state for different parameters. The different colors correspond to different values of the particle density  $\phi$ . The panels correspond to different values of the tumbling probability  $\alpha$  as indicated above each panel. Color-code:  $\phi = 0.80$  - black,  $\phi = 0.50$  - red,  $\phi = 0.20$  - blue,  $\phi = 0.07$  - green. Solid lines correspond to the expected correlations for a single cluster (coarsened regime) while the points correspond to actual measurements.

gregation dynamics of run-and-tumble particles mainly caused by collective motion. The main conclusion of this work is thus that alignment or attractive interactions are not a necessary condition for self-aggregation and phase-separation to emerge if collective motion of aggregated structures is present. Further work is however needed to better characterize and understand the implications of cluster motility on different kinds of bacterial systems. In particular, it would be interesting to explore the interplay between this mobility and attractive or aligning interactions, which would certainly yield a more realistic description of the dynamics and formation of swarming clusters in bacterial communities.

## V. ACKNOWLEDGEMENTS

We acknowledge fruitful discussion with R. Soto during the early stages of this research. This work is supported by the Spanish Ministerio de Economía y Competitividad, grant number FIS 2019... (for C.V.), grant number FIS... (for I.P.) and FIS2017-83709-R (for R.B.). I.P. acknowledges support from MINECO (Grant No. PGC2018-098373-B-I00), DURSI (Grant No. 2017SGR-884), and SNF Project No. 200021-175719

## VI. APPENDIX

### A. Steady state check

As discussed throughout this work, the fact that the system reaches a steady state is of the utmost importance for the reliability of the results. In this section we present two ways we have explored to assert that the results indeed correspond to a steady state regime.

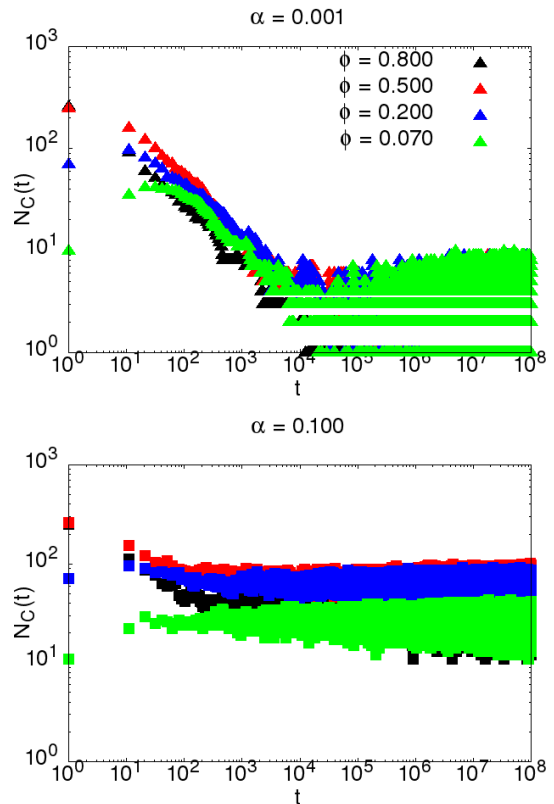


FIG. 9. Time evolution (in log-log scale) of the total number of clusters in the system for different parameters. Each panel corresponds to a fixed tumble probability  $\alpha$ , which increases from top to bottom, and varying density  $\phi$  (see legend of top panel).

The first proof that we present is the stabilization of the total number of clusters  $N_C(t) = \sum_l n_{l,t}$  around a

constant value before  $t = 10^4$  for all explored sets of parameters. Indeed, as presented in Fig.9, depending on the values of  $\phi$  and  $\alpha$ ,  $N_C(t)$  will drop for a varying number of iterations but will always end up fluctuating around a constant value. Moreover, the steady state number of clusters  $N_C = \langle N_C(t \rightarrow \infty) \rangle$  presents a consistent behavior with the state of aggregation dependence on  $\phi$  and  $\alpha$ . Indeed, for parameter sets that lead to a clustering state  $N_C$  stays high while for parameter sets corresponding to a coarsening state  $N_C$  drops very low, sometimes even reaching 1.

In an attempt to check whether the single-seed statistics used for the results presented in this work were correct, here we compare them to multi-seed statistics of the same systems. Indeed, for this work we have initialized the system only once for each set of parameters and let it run long enough to have good statistics of the steady state in a single run. Another possible way of doing it would be to measure only once in the steady state and then reinitialize the system with an independent random configuration. This would guarantee independent measurement points to average over, leading to more reliable results, but it is also a much more expensive approach from a computational point of view as the relaxation time can be very long. Since for the results presented in this work we have restricted ourselves to the former approach for full parameter sets sweeps, in this section we compare the results of both approaches for a few cases to justify our decision (see Fig.10).

In Fig.10 we present the resulting cluster size distribution for single-seed and multiple-seed statistics for the different states of aggregation of the system. We thus observe that independently of the parameter choice ( $\alpha$  and  $\phi$ ) the cluster size distribution presents consistently the same behavior for all different regimes. Note in particular how coherent the shape of the curves are, almost completely overlapping in all cases. One important feature that we observe here is also the fact that single-seed statistics present more noise in the coarsened state (see panel a)). This noise doesn't however justify choosing multiple-seed statistics over single-seed statistics for full parameter sweeps as they are much more costly computationally.

### B. Finite size effect

While coarsening is inherently a finite size effect and cannot occur for infinitely large systems, in our work we

are interested in checking that the statistics of the different states of aggregation are independent of the system's size. This means that while coarsening for a system of  $L = 2000$  will imply a maximum cluster size two times larger than for  $L = 1000$ , we expect the cluster size distribution to follow the same (or similar) law. We thus check that the cluster size distribution of the system is independent of its size in the range where we work simulating three systems of  $L = 1000$ ,  $L = 2000$  and  $L = 5000$  for different parameter sets ( $\alpha$ - $\phi$ ) and compared the resulting steady state cluster size distribution (see Fig.11).

In Fig.11 we present the resulting cluster size distribution for systems of sizes  $L = 1000$  (black circles),  $L = 2000$  (red triangles) and  $L = 5000$  (blue diamonds) and two different combinations of  $\alpha$  and  $\phi$ , corresponding to the coarsening (left panel) and clustering (right panel) regimes. Note that in the top panel we normalize the cluster size (as in Fig.4 and Fig.5) so that the two can overlap, as the maximum cluster size depends on the size of the system. For the bottom panel, however, we plot the distribution function against the real cluster size as the decay should only depend on  $\alpha$  and  $\phi$  but not on  $L$ . This is indeed what we observe, with a perfect match between the different curves for the clustering regime and a very similar and overlapping shape for the coarsening regime, with only a few statistical error differences between them (see points for intermediate sizes). We can therefore conclude that the system indeed behaves in the same way independently of  $L$  in this range of values. Note however that as the system gets larger the relaxation time for the coarsened states also increases as more particles need to merge together. This explains the higher statistical noise observed for the blue curve in the top panel. For this reason, we choose to work with  $L = 2000$  and not with larger systems, since the computational cost would be too high to achieve good statistics. We haven't worked with lower system sizes either to guarantee that all typical cluster sizes can be reached with this system for the chosen range of  $\alpha$  and  $\phi$ .

- 
- [1] S. Ramaswamy, Annual Review of Condensed Matter Physics **1**, 323 (2010), <https://doi.org/10.1146/annurev-commatphys-070909-104101>.  
 [2] G. D. Magistris and D. Marenduzzo, Physica A: Statistical Mechanics and its Applications **418**, 65 (2015), proceedings of the 13th International Summer School on

- Fundamental Problems in Statistical Physics.  
 [3] M. C. Marchetti, J. F. Joanny, S. Ramaswamy, T. B. Liverpool, J. Prost, M. Rao, and R. A. Simha, Rev. Mod. Phys. **85**, 1143 (2013).  
 [4] A. Zottl and H. Stark, Journal of Physics: Condensed Matter **28** (2016).

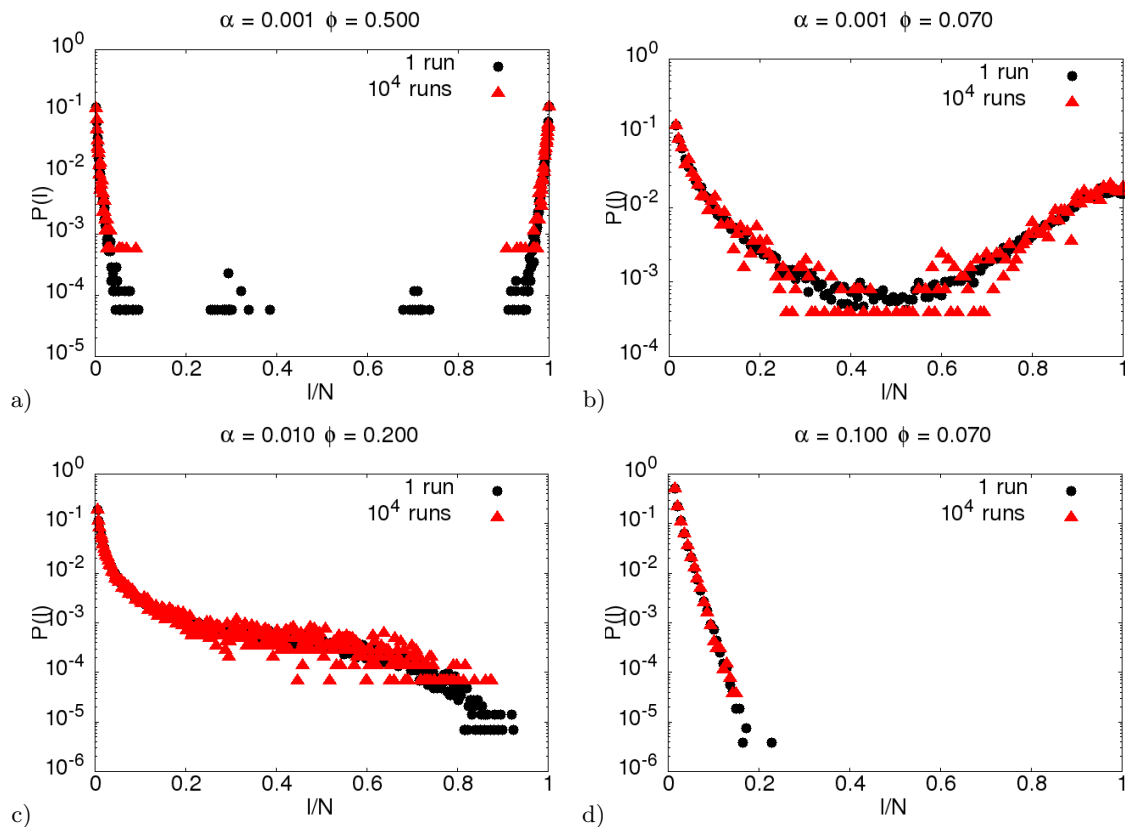


FIG. 10. Cluster size distribution as measured with single seed statistics (black circles) and with multiple seed statistics (red triangles) for different combinations of the  $\alpha$  and  $\phi$  parameters covering all different regimes. Panel a): coarsening regime. Panels b) and c): transition regime. Panel d): clustering regime. In all cases  $L = 2000$ .

- [5] S. A. Mallory, C. Valeriani, and A. Cacciuto, Annual Review of Physical Chemistry **69**, 59 (2018), pMID: 29106809, <https://doi.org/10.1146/annurev-physchem-050317-021237>.
- [6] J. Stenhammar, D. Marenduzzo, R. J. Allen, and M. E. Cates, Soft Matter **10**, 1489 (2014).
- [7] B. M. Mognetti, A. Šarić, S. Angioletti-Uberti, A. Cacciuto, C. Valeriani, and D. Frenkel, Phys. Rev. Lett. **111**, 245702 (2013).
- [8] G. S. Redner, A. Baskaran, and M. F. Hagan, Phys. Rev. E **88**, 012305 (2013).
- [9] G. S. Redner, M. F. Hagan, and A. Baskaran, Phys. Rev. Lett. **110**, 055701 (2013).
- [10] A. Suma, G. Gonnella, D. Marenduzzo, and E. Orlandini, EPL (Europhysics Letters) **108** (2014).
- [11] M. E. Cates, D. Marenduzzo, I. Pagonabarraga, and J. Tailleur, Proceedings of the National Academy of Sciences **107**, 11715 (2010), <https://www.pnas.org/content/107/26/11715.full.pdf>.
- [12] G. Delphine, D. Martin, J. Tailleur, and D. Bartolo, Phys. Rev. X **9**, 031043 (2019).
- [13] D. B. H. C. J. T. A. P. Solon, J.-B. Caussin, Phys. Rev. E **92**, 062111 (2015).
- [14] V. A. Martinez, J. Schwarz-Linek, M. Reufer, L. G. Wilson, A. N. Morozov, and W. C. K. Poon, Proceedings of the National Academy of Sciences **111**, 17771 (2014), <https://www.pnas.org/content/111/50/17771.full.pdf>.
- [15] R. Portela, P. L. Almeida, R. G. Sobral, and C. R. Leal, The European Physical Journal E **42**, 26 (2019).
- [16] G. Negro, L. N. Carenza, A. Lamura, A. Tiribocchi, and G. Gonnella, Soft Matter **15**, 8251 (2019).
- [17] Y. K. V. L. J. T. E. Woillez, Y. Zhao, Phys. Rev. Lett. **122**, 258001 (2019).
- [18] M. E. C. R. L. J. J. T. T. Nemoto, E. Fodor, Phys. Rev. E **99**, 022605 (2019).
- [19] M. E. C. Y. K. J. T. A. P. Solon, J. Stenhammar, New Journal of Physics **20**, 075001 (2018).
- [20] M. E. C. J. T. P. V. F. v. W. E. Fodor, C. Nardini, Phys. Rev. Lett. **117**, 038103 (2016).
- [21] T. Vicsek, A. Czirók, E. Ben-Jacob, I. Cohen, and O. Shochet, Phys. Rev. Lett. **75**, 1226 (1995).
- [22] T. Vicsek and A. Zafeiris, Physics Reports **517**, 71 (2012).
- [23] J. Tailleur and M. E. Cates, Physical review letters, **100**, 218103 (2008).
- [24] M. E. Cates and J. Tailleur, Annual Review of Condensed Matter Physics **6**, 219 (2015), <https://doi.org/10.1146/annurev-conmatphys-031214-014710>.
- [25] R. Soto and R. Golestanian, Physical review. E, Statistical, nonlinear, and soft matter physics, **89**, 012706 (2014).
- [26] N. Sepulveda and R. Soto, Physical Review E, **94** (2016).
- [27] N. Sepulveda and R. Soto, Physical Review Letters, **119** (2017).
- [28] A. Martn-Gmez, D. Levis, A. Daz-Guilera, and I. Pago-

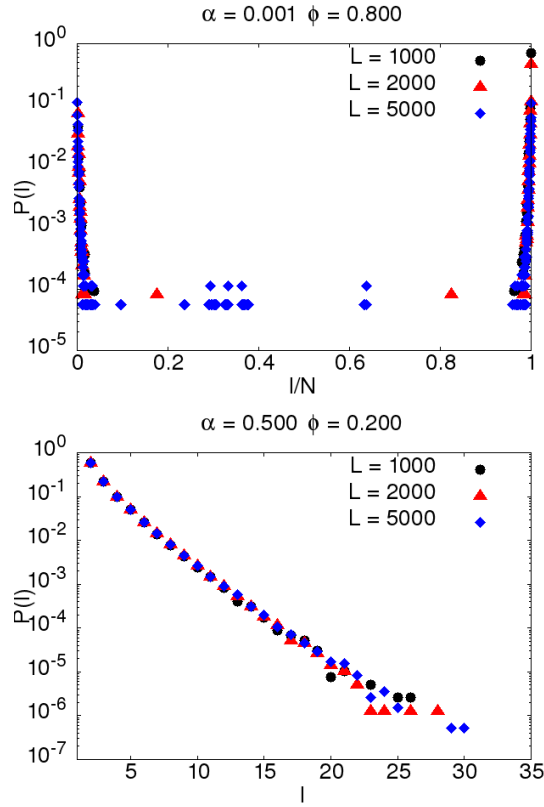


FIG. 11. Cluster size distribution as measured for different system sizes (see legends) for different combinations of the  $\alpha$  and  $\phi$  parameters covering all different regimes. Top panel: coarsening regime. Bottom panel: clustering regime. Note that the x-axis corresponds to the normalized cluster size  $l/N$  for the top panel while on the bottom panel it corresponds to the real cluster size  $l$ .

- nabarraga, *Soft Matter* **14**, 2610 (2018).
- [29] L. Barberis and F. Peruani, *The Journal of Chemical Physics* **150**, 144905 (2019), <https://doi.org/10.1063/1.5085840>.
- [30] N. C. Darnton, L. Turner, M. E. Cates, S. Rojevsky, and H. C. Berg, *Biophysical Journal* **98**, 2082 (2010).
- [31] S. E. Leggett, Z. J. Neronha, D. Bhaskar, J. Y. Sim, T. M. Perdikari, and I. Y. Wong, *Proceedings of the National Academy of Sciences* **116**, 17298 (2019), <https://www.pnas.org/content/116/35/17298.full.pdf>.
- [32] P. Illien, C. de Blois, M. N. van der Linden, and O. Dauchot, arXiv:1910.00525 (2019).
- [33] P. Greulich, L. Ciandrini, R. J. Allen, and M. C. Romano, *Phys. Rev. E* **85**, 011142 (2012).